Urban Resilience and Earthquake Engineering

ISSN: (Print) (Online) Journal homepage: www.tandfonline.com/journals/ture20

Approaching input energy spectrum from acceleration response spectrum

Longfei You, Haizhong Zhang & Yan-Gang Zhao

To cite this article: Longfei You, Haizhong Zhang & Yan-Gang Zhao (30 Apr 2025): Approaching input energy spectrum from acceleration response spectrum, Urban Resilience and Earthquake Engineering, DOI: 10.1080/30656680.2025.2480861

To link to this article: https://doi.org/10.1080/30656680.2025.2480861

Published online: 30 Apr 2025.

URBAN RESILIENCE AND EARTHQUAKE ENGINEERING
https://doi.org/10.1080/30656680.2025.2480861

Taylor & Francis
Taylor & Francis Group

RESEARCH ARTICLE

Approaching input energy spectrum from acceleration response spectrum

Longfei You[a], Haizhong Zhang[b] and Yan-Gang Zhao[a]

[a]Key Laboratory of Urban Security and Disaster Engineering of Ministry of Education, Beijing University of Technology, Beijing, People's Republic of China; [b]Eco-Science Course, Faculty of Agriculture, Yamagata University, Yamagata, Japan

ABSTRACT

The input-energy spectrum is important in energy-based seismic designs. However, most seismic design codes – such as the Chinese GB 50011-2010 and the Japanese seismic design code – only provide an acceleration response spectrum. The main objective of this study is to propose a convention model for obtaining the input energy spectrum from the acceleration response spectrum. First, a theoretical expression for the relationship between the input energy spectrum and acceleration response spectrum was proposed based on random vibration theory. Second, based on the derived theoretical expression, the impacts of various seismological parameters, including magnitude and distance, as well as structural parameters such as structural period and damping ratio on the relationship between the acceleration response spectrum and input energy spectrum were systematically explored. Finally, a practical formulation for calculating the input energy spectrum from the acceleration response spectrum (considering these seismological and structural parameters) was developed using 16,660 earthquake records from Japan. This formulation facilitates the application of energy-based design methods, enhancing their practicality for engineering applications.

ARTICLE HISTORY
Received 19 February 2025
Accepted 13 March 2025

KEYWORDS
Energy-based seismic design; input energy spectrum; acceleration response spectrum; random vibration theory; practical formulation

1. Introduction

Commonly, structural seismic design includes maximum force- and displacement-based methods. Both methods play an essential role in seismic design and are widely used; however, structural damage depends on the historical characteristics of seismic excitation in addition to the maximum force or displacement. Even if the maximum force or displacement does not exceed the threshold of the specified design, the structure may suffer cumulative damage if the input earthquake energy cannot be dissipated promptly. Maximum force- or displacement-based methods do not consider energy dissipation and accumulated damage.

To overcome these difficulties, Choi and Kim (2006) introduced an energy-based seismic design (EBSD) methodology. This methodology was initially proposed by

CONTACT Haizhong Zhang zhang@tds1.tr.yamagata-u.ac.jp Eco-Science Course, Faculty of Agriculture, Yamagata University, 1-23, Wakaba-machi, Tsuruoka-shi, Yamagata 997-8555, Japan

Housner (1956) in the 1950s and subsequently attracted considerable attention (Habibi et al. 2013). The basic concept of EBSD is that if the input earthquake energy exceeds the energy-dissipation capacity of the structure, the structure is likely to fail; otherwise, the structure is safe.

The prerequisite to EBSD is determination of the earthquake energy incident on the structure. Many scholars (Kuwamura and Galambos 1989; Decanini and Mollaioli 1998; Decanini and Mollaioli 2001; Kunnath and Chai 2004; Vahdani et al. 2019) have adopted the input energy spectrum (E_I) to characterise the earthquake energy incident on structures. To exclude the effects of the mass of the structure, E_I is typically expressed in terms of energy equivalent velocity spectrum V_{eq} ($V_{eq} = \sqrt{2E_I/m}$). However, many seismic codes (such as GB 50011 (2010) and The Building Standard Law of Japan (2016)) worldwide typically adopt the acceleration response spectrum (SA) to represent the ground motion input and do not provide V_{eq} for design. Although the V_{eq} for EBSD can be obtained based on probabilistic seismic hazard analysis (PSHA) − considering multiple potential seismic sources and various uncertainties (Merz et al. 2009) − the process is excessively complex. Deriving the V_{eq} from SA is a shortcut, circumventing complex calculation processes.

Chapman (1999) discussed the relationship between the pseudo velocity spectrum (PSV) and V_{eq}, using data from 23 earthquakes in western America. Alıcı and Sucuoğlu (2016) developed a model for V_{eq}/PSV using 104 earthquake records from a next-generation attenuation database. Akiyama and Kitamura (2006) explored the relationship between the spectrum velocity (RS_v) and V_{eq}; they proposed a simple formulation for V_{eq}/RS_v based on the harmonic seismic response. Zhang and Zhao (2023) analyzed the relationship between PSV and V_{eq} based on the random vibration theory (RVT) and developed a formulation for V_{eq}/PSV based on 16,660 seismic records from Japan. Du et al. (2020) theoretically established a conversion model between the pseudo spectral acceleration (PSA) and V_{eq} by analyzing seismic responses of single-degree-of-freedom (SDOF) systems in the frequency domain.

These studies have made significant contributions to clarifying the relationships between several types of response spectra and V_{eq}. However, there is no established conversion model from SA to V_{eq}. Many seismic design codes, such as the Chinese GB 50010 - 2010 and the Japanese seismic design code, provide only SA without corresponding PSA. Additionally, numerous studies have highlighted that PSA can be significant different from SA in many cases (Liu et al. 2025). As a result, even though conversion models from PSA to V_{eq} exist, they cannot be applied to derive V_{eq} from SA. Therefore, it is necessary to develop a conversion model specifically for transforming SA to V_{eq}.

The remainder of this paper is organised as follows: Section 2 reviews existing formulations for the relationship between V_{eq} and various response spectra. Section 3 derives a theoretical expression for V_{eq}/SA based on the RVT. Section 4 validates the feasibility of the proposed method by comparison with a time-series analysis method. Section 5 explores the effects of the structural period, damping ratio, magnitude, and distance on V_{eq}/SA. Section 6 proposes a practical V_{eq}/SA formulation using 16,660 actual seismic records from Japan. Finally, Section 7 summarises the main conclusions of this study.

2. Existing formulations for the relationship between various response spectra and energy equivalent velocity spectrum

This section offers a concise overview of existing formulations for the relationship between different response spectra and V_{eq}. Alıcı and Sucuoğlu (2016) developed a formulation for the relationship between PSV and V_{eq} based on a statistical analysis of 104 earthquakes recorded in the next-generation attenuation database. This database is a comprehensive ground motion prediction repository developed through the Pacific Earthquake Engineering Research Center initiatives (Ancheta et al. 2014). This formulation is expressed as follows:

$$\frac{V_{eq}(T_0, \xi)}{PSV(T_0, \xi)} = a \cdot e^{-bT_0} + c \tag{1}$$

where T_0 denotes the fundamental period of the SDOF oscillator, ξ represents the oscillator damping ratio; a, b and c are the regression coefficients related to T_0 and ξ.

Akiyama and Kitamura (2006) proposed a simple formulation for V_{eq}/RS_v based on a simple-harmonic seismic response, which is expressed as follows:

$$\frac{V_{eq}(\xi = 0.1)}{RS_v(\xi)} = \sqrt{C_{ak}} \times \sqrt{1 + 12\pi\xi} \tag{2}$$

where C_{ak} is an empirical coefficient – obtained from the artificial and recorded ground motions – expressed as follows:

$$C_{ak} = 1, \text{ when } D_{gm} < 50s \tag{3}$$

$$C_{ak} = 1 + 0.017(D_{gm} - 50), \text{ when } D_{gm} \geq 50s \tag{4}$$

where D_{gm} denotes the ground motion duration.

Du et al. (2020) theoretically established a direct relationship between PSA and V_{eq} by analysing the frequency-domain behaviour of an SDOF system. This relationship is expressed as follows:

$$\frac{V_{eq}(T_0, \xi)}{PSA(T_0, \xi)} = \frac{2\sqrt{\pi\xi}}{C\omega_0} \tag{5}$$

where C is a parameter that depends on the characteristics of a specific ground motion and ω_0 is the circular frequency of the SDOF oscillator. Du et al. (2020) provided the values of C for four groups.

Zhang and Zhao (2023) proposed a formulation for calculating V_{eq}/PSV and considered the effects of magnitude, distance, and site conditions using 16660 actual earthquake records in Japan, which is expressed as follows:

$$\frac{V_{eq}(T_0, 5\%)}{PSV(T_0, 5\%)} = C_{z1}T_0^2 + C_{z2}T_0^2 + C_{z3} \tag{6}$$

where C_{z1},C_{z2}, and C_{z3} are the regression coefficients related to site conditions, magnitude, and distance, respectively.

In summary, V_{eq} can be directly derived from several types of response spectra. However, there is no established conversion model from SA to V_{eq}. Many seismic

design codes, such as the Chinese GB 50010 - 2010 and the Japanese seismic design code, provide only SA. Therefore, to simply obtain V_{eq} from the SA, it is necessary to develop a SA-to- V_{eq} conversion model.

3. A theoretical expression for the ratio of input energy spectrum and acceleration response spectrum

To clarify the relationship between SA and V_{eq}, and investigate which parameters should be incorporated in the conversion model between SA and V_{eq}, a theoretical expression for V_{eq}/SA is derived in this section.

3.1. Theoretical expression for SA

Based on the RVT, SA can be obtained from the Fourier amplitude spectrum (FAS) of the acceleration response of an SDOF oscillator, expressed as follows:

$$SA(\omega_0, \xi) = pf\sqrt{\frac{1}{D_{rms}\pi}\int_0^\infty |f(\omega)|^2 |H_{sa}(\omega_0, \omega, \xi)|^2 d\omega} \tag{7}$$

where $f(\omega)$ is the FAS of the ground motion, ω is the circular frequency, and D_{rms} is the duration of the root mean square (RMS) of the oscillator response. $H_{sa}(\omega)$ denotes the oscillator transfer function for acceleration (Ohsaki 1996) and is expressed as follows:

$$|H_{sa}(\omega_0, \omega, \xi)| = -\frac{\sqrt{2\xi\omega/\omega_0{}^2 + 1}}{\sqrt{(2\xi\omega/\omega_0)^2 + ((\omega/\omega_0)^2 - 1)^2}} \tag{8}$$

The transfer function $H_{sa}(\omega)$ expressed by Eq. (8) applies to a linear SDOF system, neglecting nonlinear effects.

In Eq. (7), pf denotes the peak factor, which is defined as the ratio of the peak to root-mean-square value of a signal. This parameter is derived from extreme value statistics and can be described by a probability distribution (Wang and Rathje 2016). The cumulative distribution function of pf was given by Vanmarcke (1975) and is expressed as follows:

$$P(pf < r) = [1 - e^{(-r^2/2)}] \times \exp\left[-2f_z \exp(-r^2/2) D_{gm} \frac{\left(1 - e^{-\delta^{1.2} r\sqrt{\pi/2}}\right)}{(1 - e^{r^2/2})}\right] \tag{9}$$

where r is a random variable represents the threshold of pf, f_z represents the zero-crossing rate, δ is a bandwidth factor, which is expressed as follows:

$$\delta = \sqrt{1 - \frac{m_1^2}{m_0 m_2}} \tag{10}$$

where m_0, m_1, and m_2 are the zeroth-order, first-order, and second-order moments of the square of the FAS, respectively; the nth-order spectral moment, m_n, for a FAS, $y(\omega)$, is

expressed as follows:

$$m_n = \frac{1}{\pi}\int_0^\infty \omega^n |y(\omega)|^2 d\omega \tag{11}$$

In Eq. (9), f_z represents the zero-crossing rate and is also related to the spectral moments, which are expressed as follows:

$$f_z = \frac{1}{2\pi}\sqrt{\frac{m_2}{m_0}} \tag{12}$$

In RVT analyses, this paper focuses on the expected value, without considering the distribution, the expected value of pf is typically used, which can be obtained by $\int_0^\infty [1 - P(pf < r)]dr$.

The RMS duration of the oscillator response, D_{rms}, in Eq. (7) is related to the ground motion duration D_{gm}, and D_{rms}/D_{gm} given by Boore and Thompson (2015) is expressed as follows:

$$\frac{D_{rms}}{D_{gm}} = \left(c_{e1} + c_{e2}\frac{1-\eta^{c_{e3}}}{1+\eta^{c_{e3}}}\right)\left[1 + \frac{c_{e4}}{2\pi\xi}\left(\frac{\eta}{1+c_{e5}\eta^{c_{e6}}}\right)^{c_{e7}}\right] \tag{13}$$

where $\eta = T_0/D_{gm}$, $c_{e1} \sim c_{e7}$ are coefficients related to M and R, given by Boore and Thompson (2015). Actually, this D_{rms} was derived to estimate PSA based on RVT. This study used the RMS duration for the PSA estimation to approximate the RMS duration for the estimation of SA based on RVT.

3.2. Theoretical expression for V_{eq}

In addition, the theoretical relationship between E_I and FAS of the ground motion is given by Ordaz et al. (2003) which is derived as follows:

$$V_{eq}(\omega_0, \xi) = \sqrt{\frac{2E_I(\omega_0, \xi)}{m}} = \sqrt{-\frac{2}{\pi}\int_0^\infty |f(\omega)|^2 Re[Hv(\omega_0, \omega, \xi)]d\omega} \tag{14}$$

where m denotes the oscillator mass; $Hv(\omega_0, \omega, \xi)$ is the oscillator transfer function for the relative velocity, which is a complex number, and its real part is as follows:

$$Re[Hv(\omega_0, \omega, \xi)] = -\frac{2\xi\omega_0\omega^2}{(\omega_0^2 - \omega^2)^2 + (2\xi\omega\omega_0)^2} \tag{15}$$

3.3. The relationship between SA and V_{eq}

To establish the relationship between SA and V_{eq}, the ratio of V_{eq} to SA can be derived from Eqs. (7) and (14). However, the dimensions of V_{eq} and SA are different: V_{eq} has the same dimension as velocity (cm/s), while SA shares the dimension of acceleration (cm/s^2). To unify the dimensions, SA is converted to a pseudo velocity spectrum, PSV_{sa}, by dividing by ω_0 ($PSV_{sa} = SA/\omega_0$) ensuring that PSV_{sa} shares the same dimension as V_{eq}. Consequently, the ratio V_{eq}/PSV_{sa} becomes dimensionless. Based on Eqs. (7) and

(14), V_{eq}/PSV_{sa} is expressed as follows:

$$\frac{V_{eq}(\omega_0, \xi)}{PSV_{sa}(\omega_0, \xi)} = \frac{V_{eq}}{SA/\omega_0} = \sqrt{\frac{\int_0^\infty |f(\omega)|^2(-Re[Hv(\omega_0, \omega, \xi)])d\omega}{\int_0^\infty |f(\omega)H_{sa}(\omega, \omega_0, \xi)/\omega_0|^2 d\omega}} \times \frac{\sqrt{2D_{rms}}}{pf} \tag{16}$$

Equation (16) successfully links SA and V_{eq}. Since this equation incorporates parameters such as magnitude, distance, structural period, and damping ratio, it can be used to explore their influence on the trend of V_{eq}/PSV_{sa}.

4. Comparison with time-series analysis

To confirm the accuracy of the expression derived in Section 3, the V_{eq}/PSV_{sa} values calculated using Eq. (16) were compared with the results obtained from the time-series analysis. To this end, a wide range of oscillator periods, T_0 (0.01–6 s), damping ratios, ξ (5%–50%), distances R (50.24–200.01 km), and magnitudes of moments, M (4–8) were considered. The FAS $f(\omega)$ used in Eq. (16) is generated based on the widely used point-source FAS model introduced by Boore (2003). The values of the seismological parameters required for this model were determined according to Boore and Thompson (2015) and were consistent with those used by Zhang and Zhao (2023). The time series for the analysis was generated from the FAS using a stochastic method simulation program (Boore 2000). For each FAS, a suite of 100 time-series signals were generated, and the simulated time series matched the FAS on average. The V_{eq}/PSV_{sa} values for the generated accelerations were computed using the direct integration method (Nigam and Jennings 1969).

The results of the derived expressions (Eq. (16)) were compared with those from the time-series analysis, and representative comparisons are shown in Figure 1, Figure 2 and Figure 3. The results of Eq. (16) agree well with those obtained from the time-series analysis. Although the relative error increased with a decrease in the damping ratio, the maximum relative error did not exceed 10%. This error may have been caused by using the RMS duration for PSA estimation to approximate the RMS duration for the SA estimation, based on the RVT, and is a subject for future research.

5. Parameter analysis

To construct a conversion model from SA to V_{eq}, the properties of V_{eq}/PSV_{sa} and the effects of various parameters on V_{eq}/PSV_{sa} are explored based on the theoretical expression derived in Section 3. Section 5.1 discusses the effects of the structural period and damping ratio on V_{eq}/PSV_{sa}, Section 5.2 discusses the effect of moment magnitude on V_{eq}/PSV_{sa}, and Section 5.3 discusses the effect of distance on V_{eq}/PSV_{sa}.

5.1. The influences of structural period and damping ratio on spectrum ratio

To explore effects of structural period and damping ratio on V_{eq}/PSV_{sa}, values of V_{eq}/PSV_{sa} for different structural periods and damping ratios are calculated, as shown in Figure 1. In the short-period range, the V_{eq}/PSV_{sa} ratio decreases rapidly with increasing the structural period. In the long-period range, the variation of V_{eq}/PSV_{sa} depends on

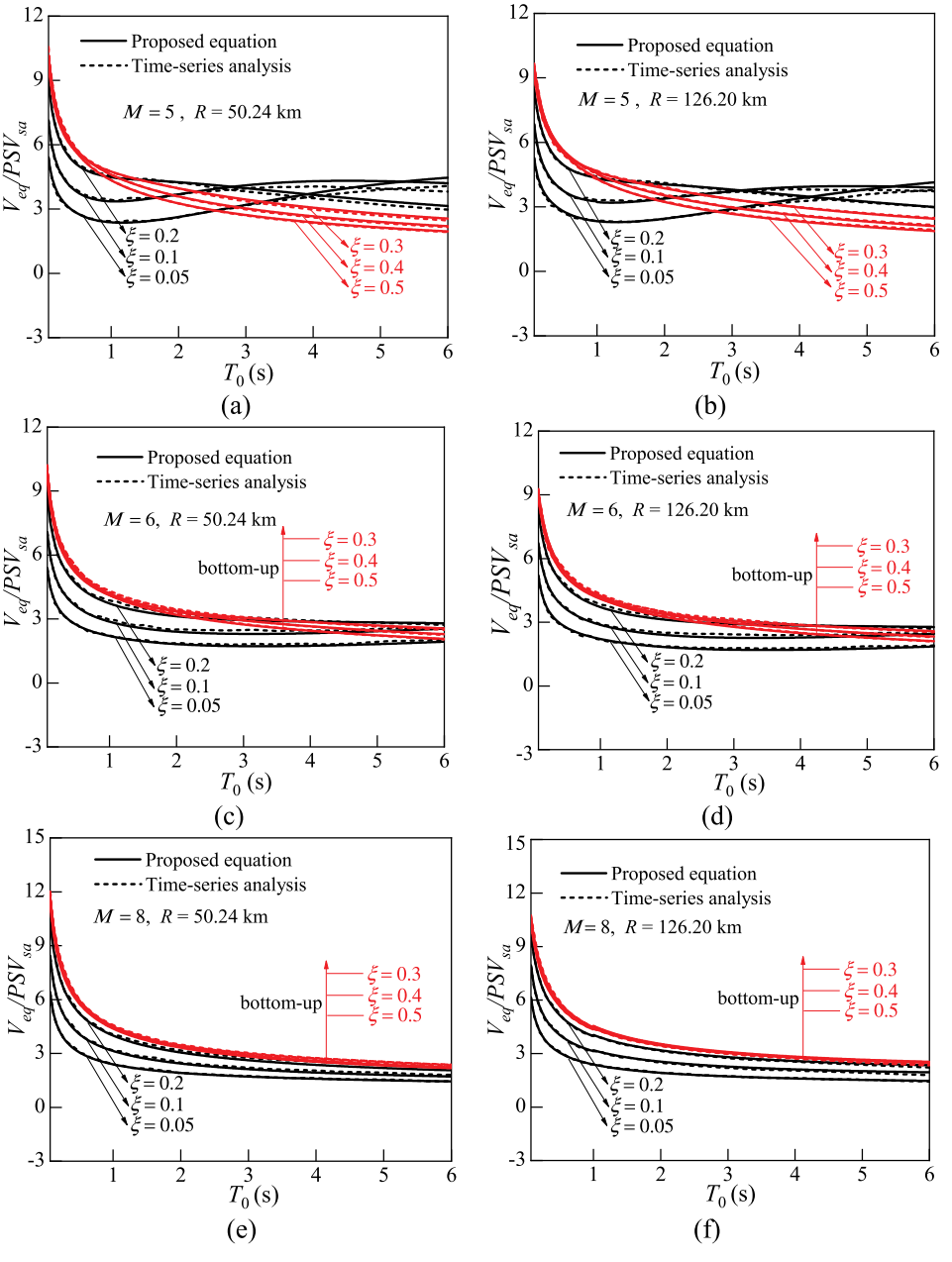

Figure 1. Comparison of the average V_{eq}/PSV_{sa} values obtained using the time-series analysis and proposed equation: (a) $R = 50.24$km, $M = 5$; (b) $R = 126.20$km, $M = 5$; (c) $R = 50.24$km, $M = 6$; (d) $R = 126.20$km, $M = 6$; (e) $R = 50.24$km, $M = 8$; and (f) $R = 126.20$km, $M = 8$.

the damping ratio and magnitude. When both the magnitude and damping ratio are small, V_{eq}/PSV_{sa} increases slowly with increasing structural period. When either the damping ratio or magnitude is large, V_{eq}/PSV_{sa} decreases slowly with increasing the structural period.

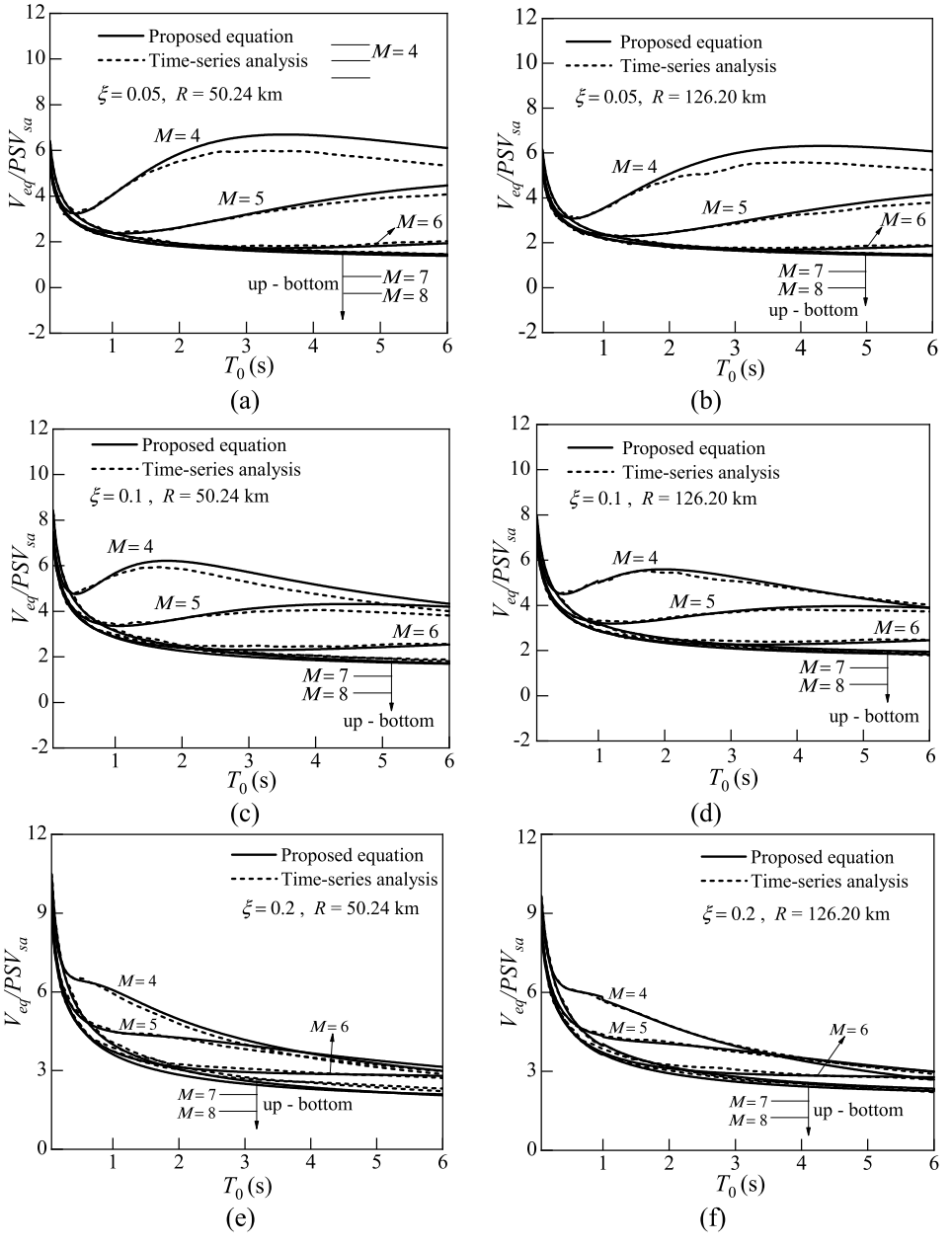

Figure 2. Comparison of V_{eq}/PSV_{sa} values obtained using the time-series analysis and proposed equation for different moment magnitudes: (a) $R = 50.24$km, $\xi = 0.05$; (b) $R = 126.20$km, $\xi = 0.05$; (c) $R = 50.24$km, $\xi = 0.1$; (d) $R = 126.20$km, $\xi = 0.1$;(e) $R = 50.24$km, $\xi = 0.2$; and (f) $R = 126.20$km, $\xi = 0.2$.

In addition, it is evident from Figure 1 that when the damping ratio is less than 0.2, V_{eq}/PSV_{sa} increases with the damping ratio in the short-period range. In the long-period range, the variation of V_{eq}/PSV_{sa} with the damping ratio depends on the magnitude. When the magnitude is large, V_{eq}/PSV_{sa} increases with the damping ratio, whereas

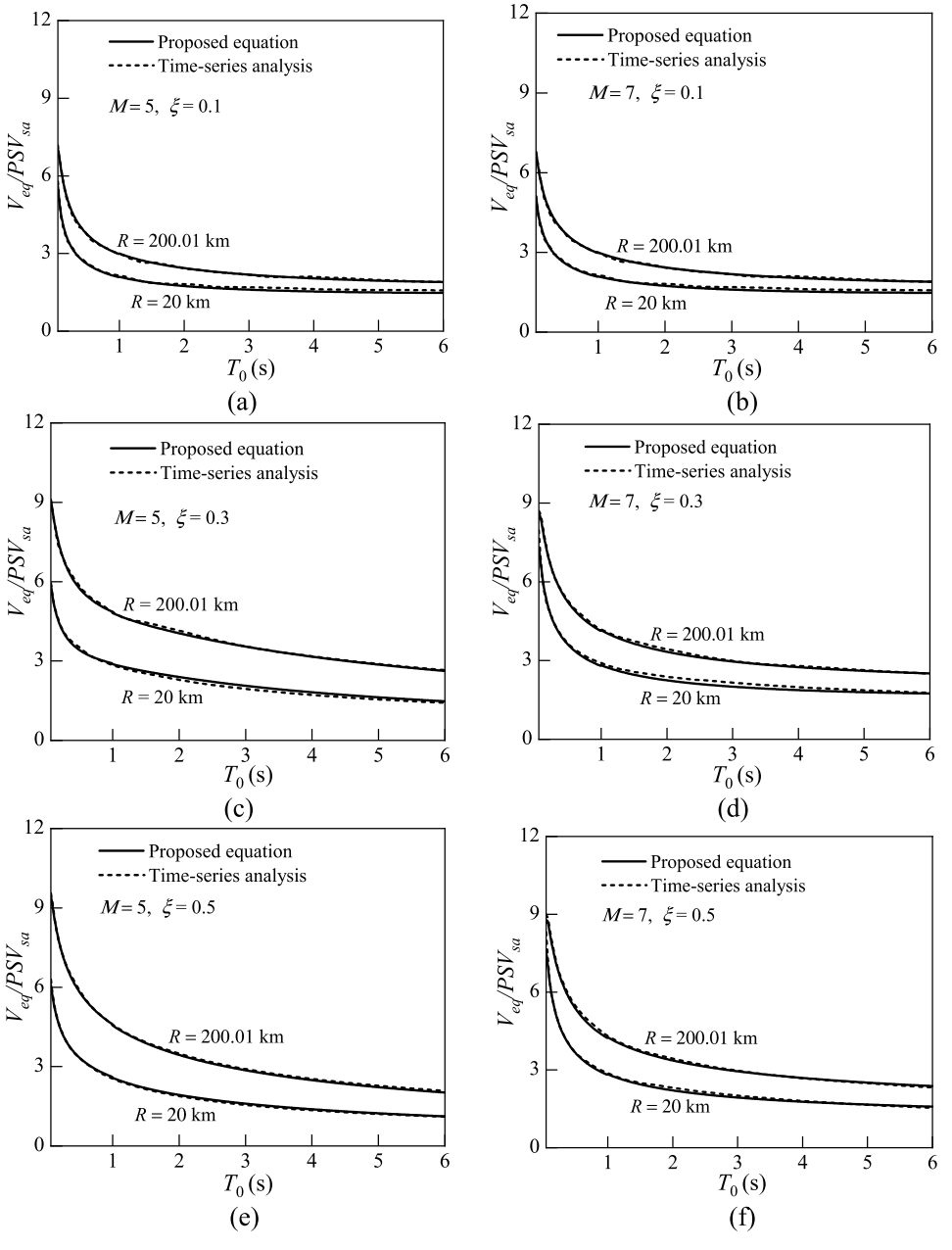

Figure 3. Comparison of the average V_{eq}/PSV_{sa} values obtained using the time-series analysis and proposed equation for different distances: (a) $\xi = 0.1, M = 5$; (b) $\xi = 0.1$, $M = 7$; (c) $\xi = 0.3$, $M = 5$; (d) $\xi = 0.3$, $M = 7$; (e) $\xi = 0.5$, $M = 5$; and (f) $\xi = 0.5$, $M = 7$.

when the magnitude is small, the variation V_{eq}/PSV_{sa} with the damping ratio is irregular. When the damping ratio exceeds 0.2, V_{eq}/PSV_{sa} decreases with an increase in the damping ratio.

5.2. The influence of moment magnitude on spectrum ratio

To explore the effect of the moment magnitude on V_{eq}/PSV_{sa}, the values of V_{eq}/PSV_{sa} for different moment magnitudes were calculated, as shown in Figure 2. It is evident from Figure 2 that in very short period range ($T_0 < 0.5$), the influence of the magnitude on V_{eq}/PSV_{sa} is minimal. In the long-period range, the variation of V_{eq}/PSV_{sa} with magnitude depends on the damping ratio. When the damping ratio is small, V_{eq}/PSV_{sa} decreases with an increasing magnitude. With an increase in the damping ratio, the variation range of V_{eq}/PSV_{sa} decreased and gradually became irregular.

5.3. The influence of distance on spectrum ratio

To explore the effect of distance on V_{eq}/PSV_{sa}, values of V_{eq}/PSV_{sa} for different distances are calculated, as shown in Figure 3. From Figure 3, it is evident that V_{eq}/PSV_{sa} increases with increasing the distance. Additionally, the distance has a minimal effect on the shape of the V_{eq}/PSV_{sa} curve.

6. A practical formulation for spectrum ratio

Section 5 indicates that V_{eq}/PSV_{sa} is affected significantly by the structural period and magnitude and moderately by the damping ratio and distance. In principle, all these parameters should be incorporated into the V_{eq}/PSV_{sa} formulation. However, seismic design codes do not explicitly specify the magnitude and distance; therefore, it is important to identify a parameter that can be obtained from seismic design and reflects the influence of magnitude and distance. Zhang and Zhao (2022) found that the magnitude and distance affect the relationship between V_{eq} and PSA by altering the shape of the spectrum. Because SA is similar to PSA, it can be inferred that the magnitude and distance also affect the relationship between V_{eq} and SA by altering the shape of the spectrum. Therefore, a response-spectrum shape factor is proposed to reflect the effects of the magnitude and distance, which is expressed as follows:

$$\zeta = \frac{SA(6s)}{PGA} \tag{17}$$

In this equation, $SA(6s)$ denotes the value of spectral acceleration at 6 s, whereas the peak ground acceleration (PGA) corresponds to the spectral acceleration at 0 s. Note that ζ can be directly obtained from the SA specified in the seismic design codes. Zhang and Zhao (2022) demonstrate that ζ is closely related to M and R, suggesting that ζ can quantify the joint effects of M and R.

To develop a practical V_{eq}/PSV_{sa} formulation, 16,660 seismic records from Japan were utilised, comprising both shallow crustal earthquakes and subduction zone earthquakes. The dataset is identical to that employed by Zhang et al. (2023), and detailed information about these ground motion records is comprehensively described in their study. The PGA of all selected records exceeded 20 gal. The Japan Meteorological Agency (JMA) magnitude M_j of the ground motions varied from $4-9$, and the epicentral distance R_e varied from $10-200$ km, as shown in Figure 4. Data were recorded at 338 stations in Japan. Specifically, 63 stations belong to site class B, 112 to site class C, 107 to site

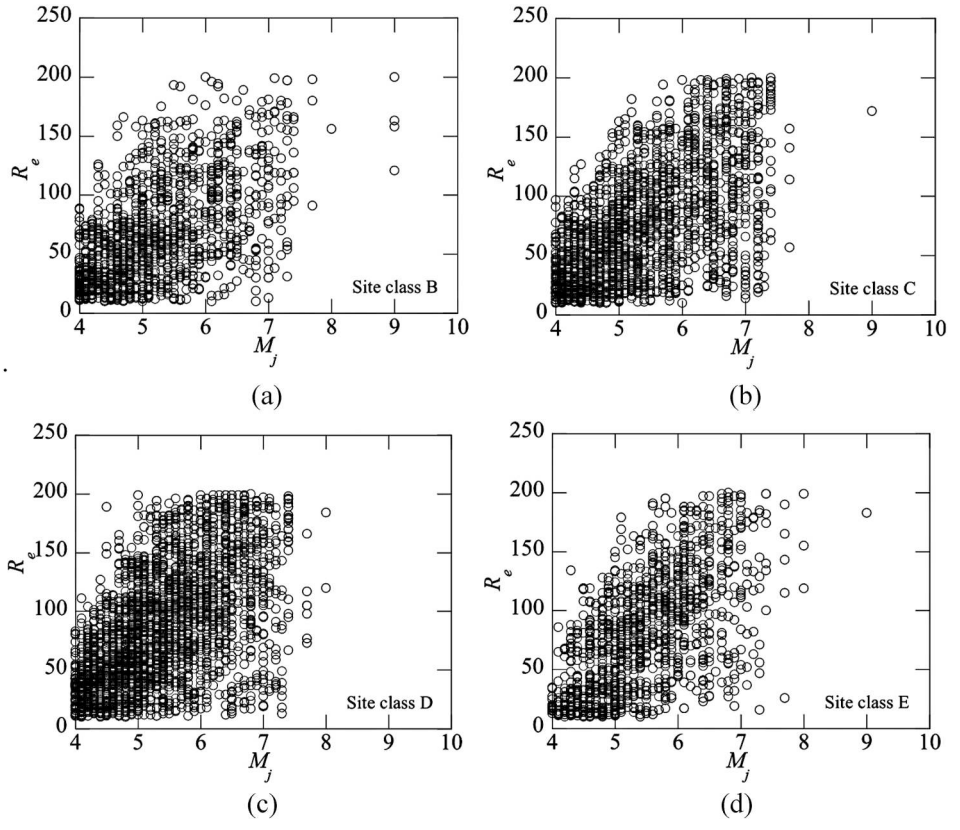

Figure 4. Distribution of Japan Meteorological Agency magnitude *Mj* and epicentral distance *Re* of ground motions recorded in site classes: (a) B; (b) C; (c) D; and (d) E.

class D, and 112 to site class E. Site classes were defined according to the National Earthquake Hazards Reduction Program (NEHRP 2000).

Notably, the types of earthquakes (e.g. shallow crustal earthquakes and subduction zone earthquakes) may influence the calculation results. Nevertheless, in most seismic codes, SA is defined without distinguishing earthquake types, using a single SA value that incorporates all earthquake categories. To maintain consistency, this study also does not differentiate between earthquake types.

In addition, the baseline of all ground-motion records was corrected to eliminate long period noise. Ideally, each ground motion record should be processed to filter out frequencies with low signal-to-noise ratios while retaining only the usable frequency range. However, as the focus of this study was the V_{eq}/PSV_{sa} ratio, it was assumed that the noise present in both V_{eq} and PSV_{sa} could be negated by calculating this ratio. To validate this assumption, the V_{eq}/PSV_{sa} results with and without the processing of the ground-motion records were compared, as shown in Figure 5. For the comparison, we selected the group in site class C with the smallest magnitudes ($4 \leq M_j < 5.5$) and the largest distances ($100 \leq R_e < 200$ km), which are likely to be affected by noise. The noise window was identified using the automatic P-phase arrival time picker developed by Kalkan (2016), and the frequencies with unacceptably low signal-to-noise ratios were

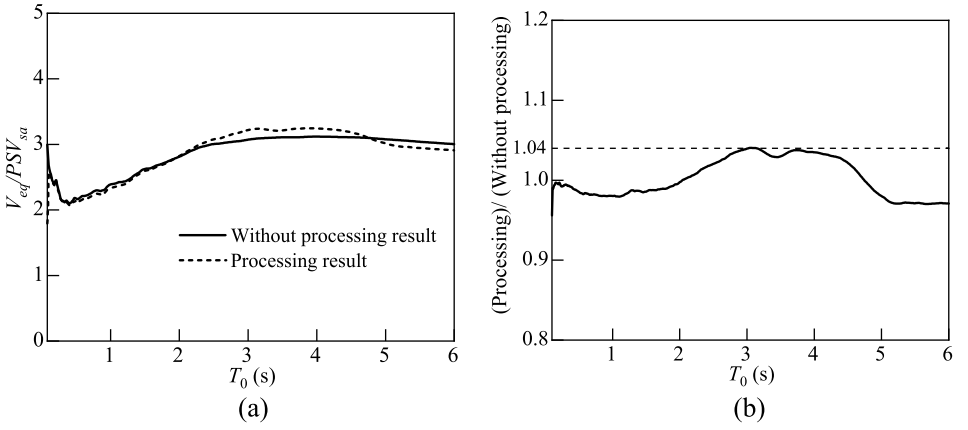

Figure 5. Comparison of V_{eq}/PSV_{sa} calculation results between those filtered for frequencies with unacceptably low signal-to-noise ratios and those without such processing. (a) Processing and without processing result; (b) The ratio of processing and without processing result.

filtered using the method proposed by Bahrampouri et al. (2021). As shown in Figure 5, there was no significant difference between the V_{eq}/PSV_{sa} results for the processed and unprocessed ground-motion records. The maximum difference between the two groups was 4%. Thus, filtering frequencies with unacceptably low signal-to-noise ratios did not significantly affect the V_{eq}/PSV_{sa} ratio. Consequently, no further processing was applied to the ground-motion records except for baseline correction.

Based on the statistical analysis of the selected seismic records, a practical V_{eq}/PSV_{sa} formulation was proposed. To obtain smooth V_{eq}/PSV_{sa} results, the selected seismic records were divided into 45 groups according to magnitude, distance, and site conditions. The equation for V_{eq}/PSV_{sa} is then expressed as follows:

$$\ln\left(\frac{V_{eq}}{PSV_{sa}}\right) = a + b\ln T_0 + ce^{-T_0} \tag{18}$$

In Eq. (18), a, b, and c are regression parameters related to the damping ratio, which are expressed as follows:

$$a = a_1\xi + a_2 \tag{19}$$

$$b = b_1\xi + b_2 \tag{20}$$

$$c = c_1\xi + c_2 \tag{21}$$

where a_1, a_2, b_1, b_2, c_1,and c_2 are the regression coefficients depending on the shape factor ζ and the site conditions provided in Appendix Tables A and B.

To verify the accuracy of the proposed V_{eq}/PSV_{sa} formulation, the V_{eq}/PSV_{sa} results derived from the formulation were compared to those obtained from real seismic records. The comparison results are shown in Figure 6, Figure 7, Figure 8 and Figure 9. From these figures, it is evident that the V_{eq}/PSV_{sa} results derived from the proposed formulation align closely with those from real seismic records, and the average error does not exceed 10%. In addition, it can be seen from Figure 6, Figure 7 and

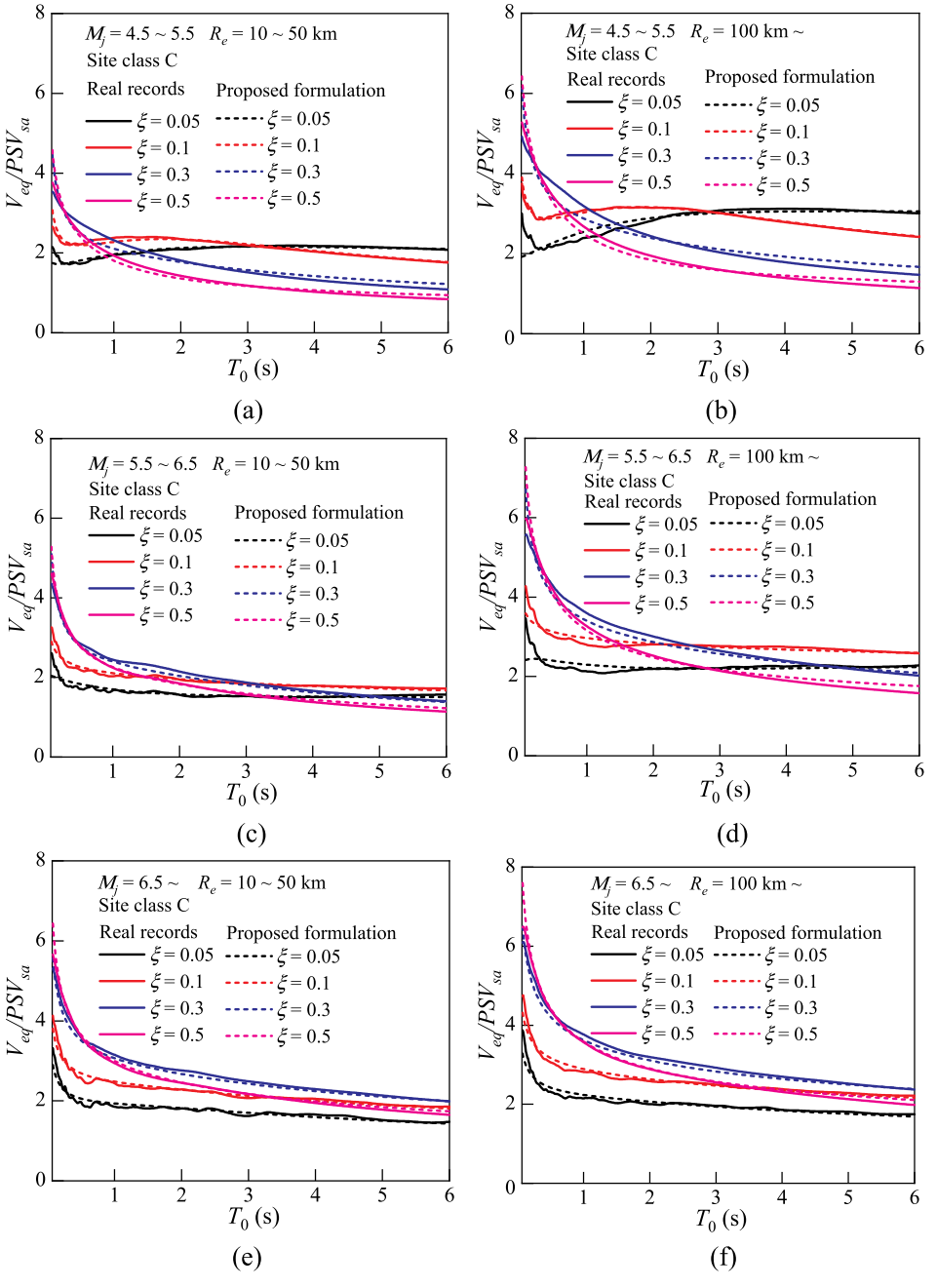

Figure 6. Comparisons of the average V_{eq}/PSV_{sa} values obtained from seismic records and proposed formulation for different ratios: (a) $R_e = 10 \sim 50$km, $M_j = 4.5 \sim 5.5$; (b) $R_e = 100$km $\sim$, $M_j = 4.5 \sim 5.5$; (c) $R_e = 10 \sim 50$km, $M_j = 5.5 \sim 6.5$; (d) $R_e = 100$km $\sim$, $M_j = 5.5 \sim 6.5$; (e) $R_e = 10 \sim 50$km, $M_j = 6.5 \sim$; (f) $R_e = 100$km $\sim$, $M_j = 6.5 \sim$.

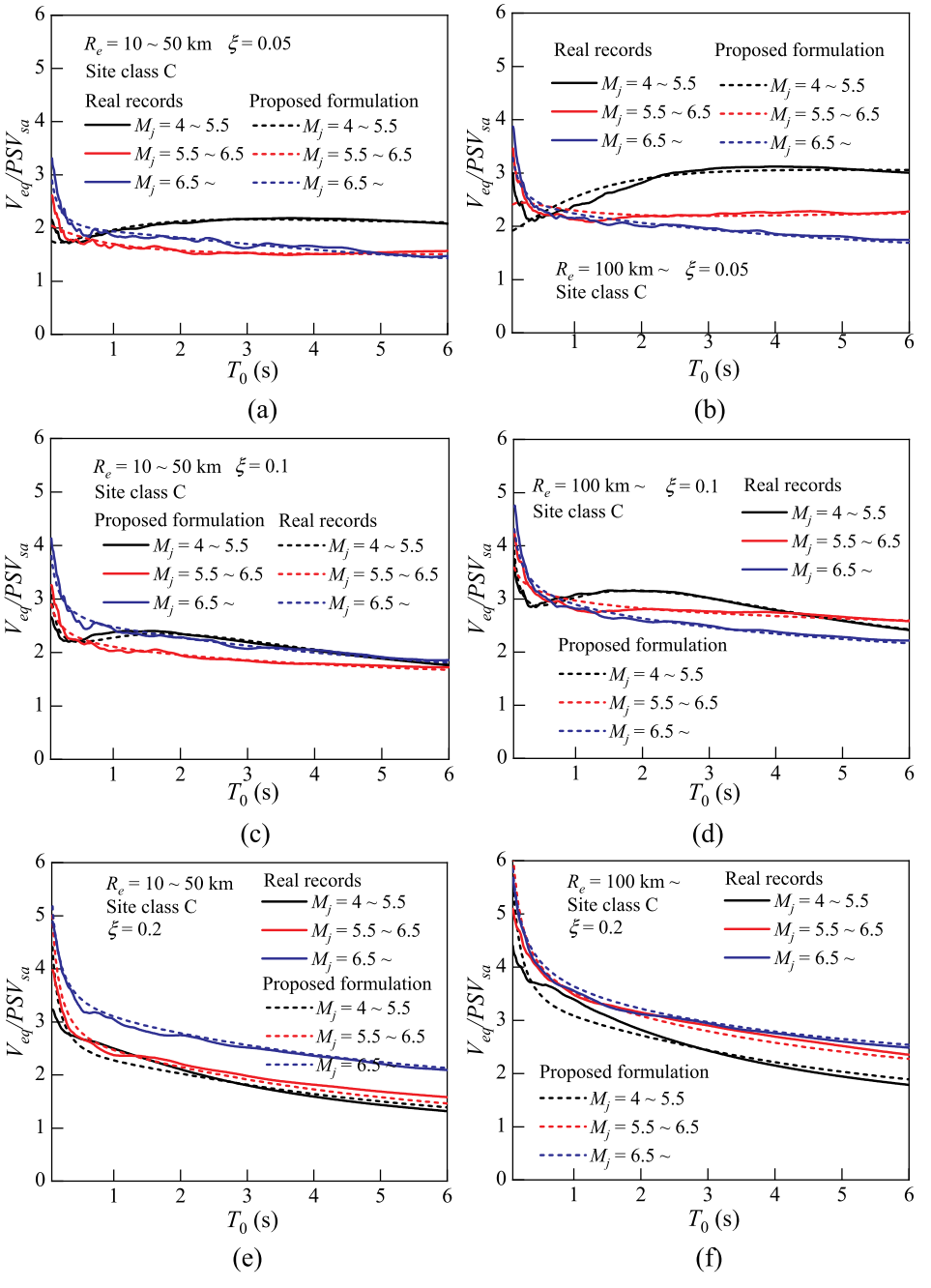

Figure 7. Comparisons of the average values obtained from seismic records and proposed formulation for different magnitudes: (a) $R_e = 10 \sim 50$ km, $\xi = 0.05$; (b) $R_e = 100$km $\sim$, $\xi = 0.05$; (c) $R_e = 10 \sim 50$km, $\xi = 0.1$; (d) $R_e = 100$km $\sim$, $\xi = 0.1$; (e) $R_e = 10 \sim 50$km, $\xi = 0.3$; (f) $R_e = 100$km $\sim$, $\xi = 0.3$.

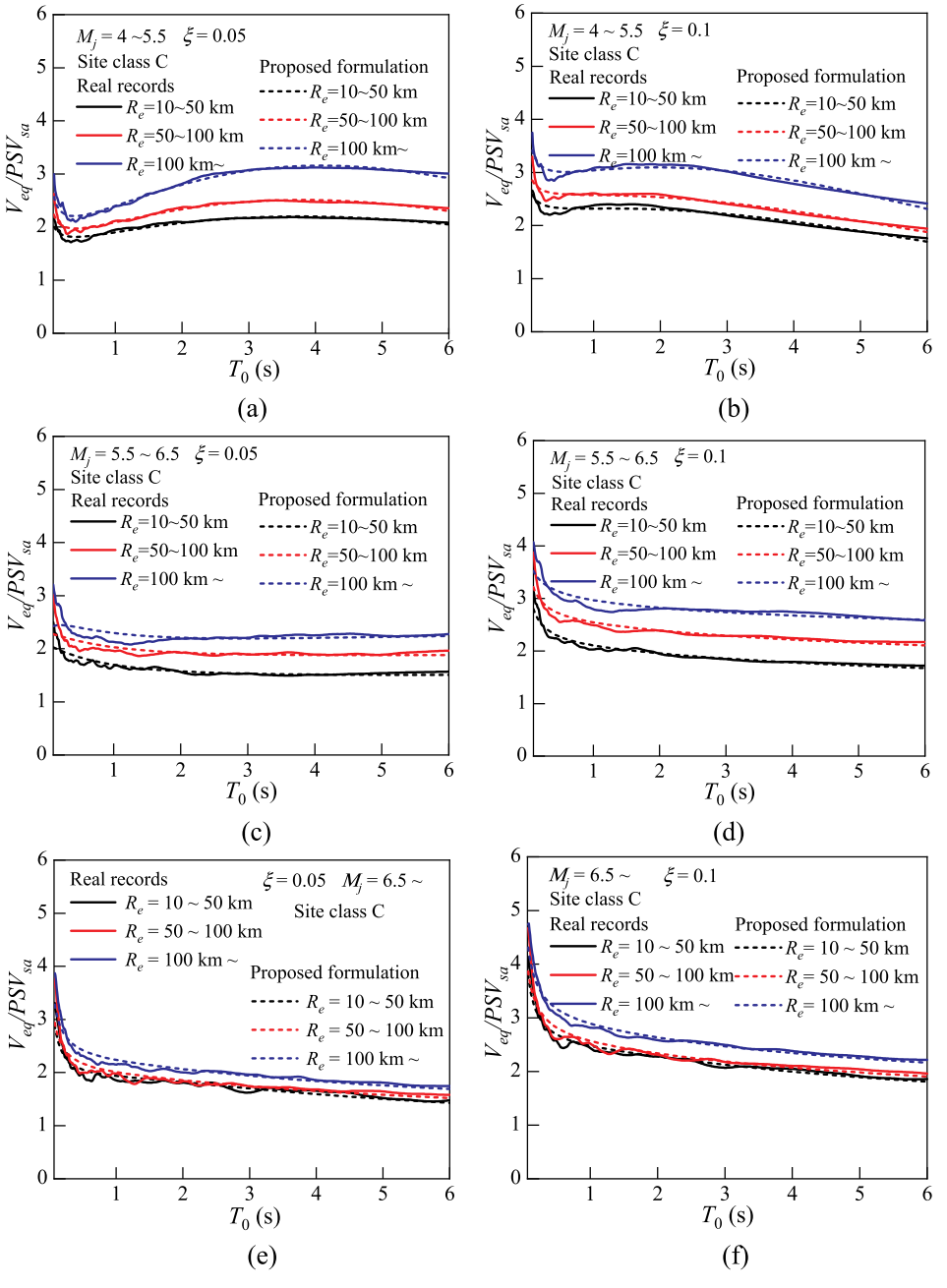

Figure 8. Comparisons of the average V_{eq}/PSV_{sa} values obtained from seismic records and proposed formulation for different distances: (a) $\xi = 0.05$, $M_j = 4 \sim 5.5$; (b) $\xi = 0.1$, $M_j = 4 \sim 5.5$; (c) $\xi = 0.05$, $M_j = 5.5 \sim 6.5$; (d) $\xi = 0.1$, $M_j = 5.5 \sim 6.5$; (e) $\xi = 0.05$, $M_j = 6.5 \sim$; (f) $\xi = 0.1$, $M_j = 6.5 \sim$.

Figure 8 that the variation in V_{eq}/PSV_{sa} with structural period, damping ratio, magnitude, and distance from real seismic records is generally consistent with those from the theoretical expression in Section 3.

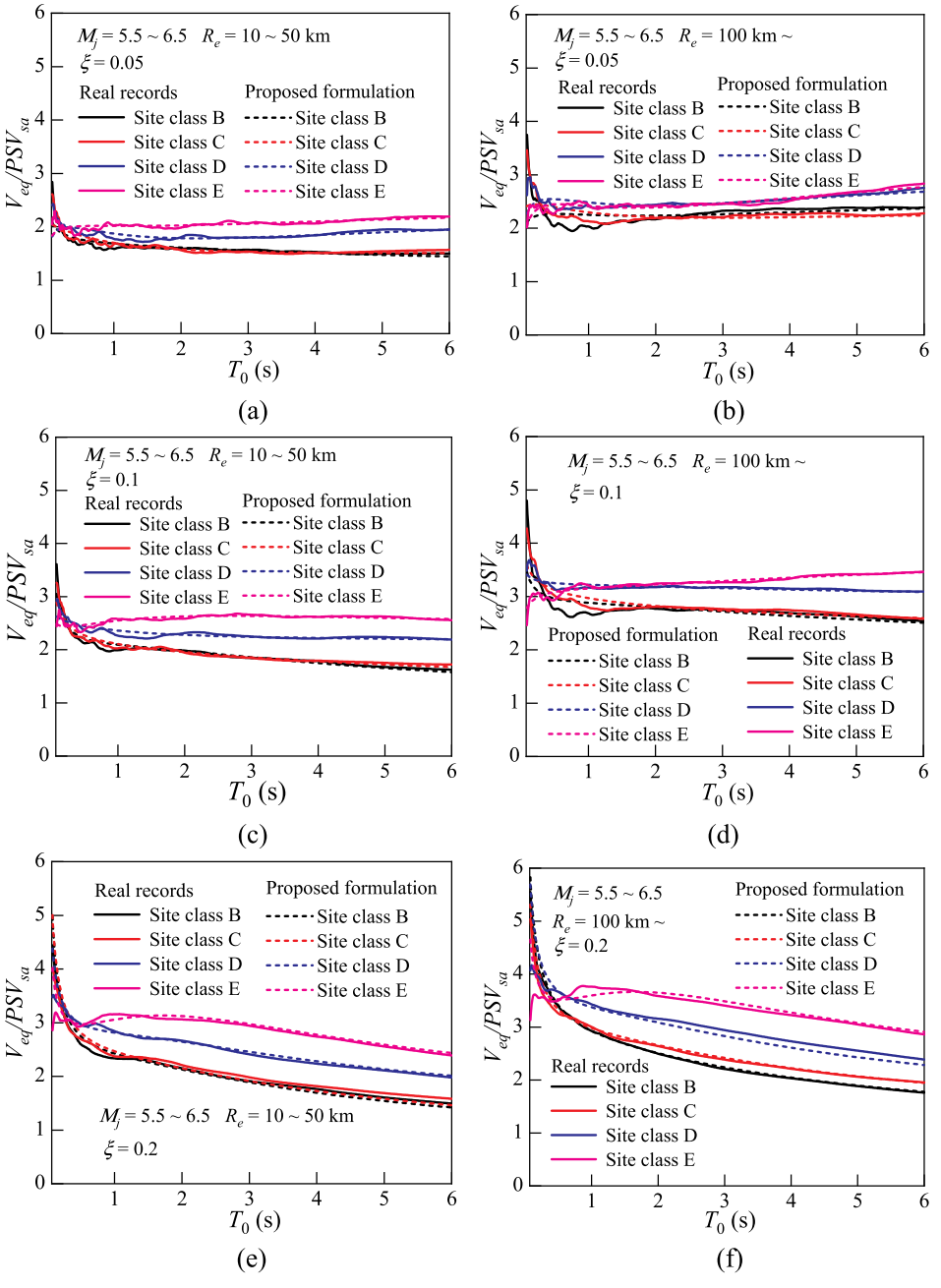

Figure 9. Comparisons of the average V_{eq}/PSV_{sa} values obtained from seismic records and proposed formulation for different sites: (a) $R_e = 10 \sim 50$ km, $\xi = 0.05$; (b) $R_e = 100$km ~, ;(c) $R_e = 10 \sim 50$km, $\xi = 0.1$; (d) $R_e = 100$km ~,$\xi = 0.1$; (e) $R_e = 10 \sim 50$km, ; (f) $R_e = 100$km ~, $\xi = 0.2$.

In addition, the site effects on V_{eq}/PSV_{sa} are not discussed in Section 5 because the proposed theoretical relationship does not involve a site class term. In this section, the effect of the site conditions on V_{eq}/PSV_{sa} is explored by comparing the results for

different site classes, as shown in Figure 9. The V_{eq}/PSV_{sa} values generally increased across most periods as the site class varied from B to E. Moreover, the variation range of V_{eq}/PSV_{sa} with the site class increased with the damping ratio.

In conclusion, Eq. (18) can potentially be employed to derive V_{eq} from SA, which is well-defined in seismic design codes, thereby directly supporting energy-based seismic design. This approach offers a simpler alternative compared to deriving V_{eq} through PSHA, as PSHA involves computationally intensive procedures and requires detailed information about seismic faults/zones and ground motion attenuation relationships. However, whether Eq. (18) provides sufficient accuracy compared to PSHA still needs to be further explored in future studies.

7. Conclusions

This study derived a theoretical expression for the relationship between the input energy spectrum and the acceleration response spectrum based on random vibration theory. Then, a practical formulation for calculating the ratio of input energy spectrum and acceleration response spectrum that considered these influences was established using 16,660 real seismic records from Japan. It is found that:

(1) The spectrum ratio calculated using the proposed theoretical expression are in good agreement with those of the time-series analysis, and the expression effectively captures the relationship between the input energy spectrum and the acceleration response spectrum, along with the observed variation trends related to magnitude, distance, structural period, and damping ratio in real seismic records.
(2) The spectrum ratio decreases rapidly with an increase in structural period in the short-period range, while in the long-period range, its variation is mainly influenced by damping ratio and magnitude. When either the damping ratio or magnitude is large, the spectrum ratio shows a downward trend with increasing structural period, whereas when both the damping ratio and magnitude are small, the spectrum ratio increases slowly. Additionally, the spectrum ratio also increases with distance, though distance has minimal effect on the shape of the spectrum ratio curve.
(3) The spectrum ratio calculated using the proposed practical formulation is in good agreement with the results obtained from real seismic records.

Although the formula proposed in this paper has the aforementioned advantages, it still exhibits the following limitations. First, the formula proposed in this paper is only applicable to SDOF systems, and the applicability to more complex structures remains to be further studied. Second, the accuracy comparison between the proposed method and the probabilistic seismic hazard analysis method are worthy of further study. Third, the seismic records utilised in this study were exclusively sourced from Japan; therefore, the applicability of the proposed model to other regions requires further investigation.

Disclosure statement

No potential conflict of interest was reported by the author(s).

Funding

This work was supported by Natural Science Foundation of China: [Grant Number 52278135].

Data availability statement

All data generated or analyzed in this study have been provided, and the doi of the data is doi:10.6084/m9.figshare.28434980.

References

Akiyama H, Kitamura H. 2006. Relationship between energy spectra and velocity response spectra. J Struct Construc Eng. 71(608):37–43. doi:10.3130/aijs.71.37_4

Alıcı FS, Sucuoğlu H. 2016. Prediction of input energy spectrum: attenuation models and velocity spectrum scaling. Earthq Eng Struct Dynam. 45(13):2137–2161. doi:10.1002/eqe.2749

Ancheta T D, Darragh R B, Stewart JP, et al. 2014. NGA-West2 database. Earthq Spectra. 30(3):989–1005. doi:10.1193/070913EQS197M

Bahrampouri M, Rodriguez-Marek A, Shahi S, et al. 2021. An updated database for ground motion parameters for KiK-net records. Earthq Spectra. 37(1):505–522. doi:10.1177/8755293020952447

Boore DM. 2000. SMSIM–Fortran programs for simulating ground motions from earthquakes: Version 2.0.–a revision of OFR 96-80-A (No. 2000-509). US Geological Survey.

Boore DM. 2003. Simulation of ground motion using the stochastic method. Pure Appl Geophys. 160(3):635–676. doi:10.1007/PL00012553

Boore D M, Thompson EM. 2015. Revisions to some parameters used in stochastic-method simulations of ground motion. Bull Seismol Soc Amer. 105(2A):1029–1041. doi:10.1785/0120140281

Chapman MC. 1999. On the use of elastic input energy for seismic hazard analysis. Earthq Spectra. 15(4):607–635. doi:10.1193/1.1586064

China Academy of Architectural Engineering. 2010. Code for seismic design of buildings (GB 50011-2010). Beijing: Ministry of Housing and Urban-Rural Development of the People's Republic of China, China Building Industry Press.

Choi H, Kim J. 2006. Energy-based seismic design of buckling-restrained braced frames using hysteretic energy spectrum. Eng Struct. 28(2):304–311. doi:10.1016/j.engstruct.2005.08.008

Decanini LD, Mollaioli F. 1998. Formulation of elastic earthquake input energy spectra. Earthq Eng Struct Dynam. 27(12):1503–1522. doi:10.1002/(SICI)1096-9845(199812)27:12<1503::AID-EQE797>3.0.CO;2-A

Decanini LD, Mollaioli F. 2001. An energy-based methodology for the assessment of seismic demand. Soil Dynam Earthq Eng. 21(2):113–137. doi:10.1016/S0267-7261(00)00102-0

Du B, He Z, Wu Y, et al. 2020. Compatible energy demand estimate considering code-specified design spectra. Soil Dynam Earthq Eng. 137(8):106273. doi:10.1016/j.soildyn.2020.106273

Habibi A, Chan R, Albermani F. 2013. Energy-based design method for seismic retrofitting with passive energy dissipation systems. Eng Struct. 46:77–86. doi:10.1016/j.engstruct.2012.07.011

Housner GW. 1956. Limit design of structures to resist earthquakes. Proceedings of the 1st World Conference on Earthquake Engineering. Berkeley, California.

Japan Building Disaster Prevention Association. 2016. The building standard law of Japan. Tokyo: Urban Building Division Housing Bureau, The Building Center of Japan.

Kalkan E. 2016. An automatic P-phase arrival-time picker. Bull Seismol Soc Amer. 106(3):971–986. doi:10.1785/0120150111

Kunnath SK, Chai YH. 2004. Cumulative damage-based inelastic cyclic demand spectrum. Earthq Eng Struct Dynam. 33(4):499–520. doi:10.1002/eqe.363

Kuwamura H, Galambos TV. 1989. Earthquake load for structural reliability. J Struct Eng. 115(6):1446–1462. doi:10.1061/(ASCE)0733-9445(1989)115:6(1446)

Liu Z, Zhao Y G, Zhang HZ. 2025. An efficient conversion model between acceleration and pseudo-acceleration response spectra considering effects of magnitude, distance, and site class. Earthq Eng Eng Vibr. 24(1):15–30. doi:10.1007/s11803-025-2292-x

Merz B, Elmer F, Thieken AH. 2009. Significance of" high probability/low damage" versus" low probability/high damage" flood events. Nat Haz Earth Syst Sci. 9(3):1033–1046. doi:10.5194/nhess-9-1033-2009

NEHRP. 2000. Recommended provisions for seismic regulations for New buildings and other structures. Washington, DC: Federal Emergency Management Agency.

Nigam NC, Jennings PC. 1969. Calculation of response spectra from strong-motion earthquake records. Bull Seismol Soc Amer. 59(2):909–922. doi:10.1785/BSSA0590020909

Ohsaki Y. 1996. Building vibration theory. Tokyo: Shokokusha Publishing Co., Ltd.

Ordaz M, Huerta B, Reinoso E. 2003. Exact computation of input-energy spectra from Fourier amplitude spectra. Earthq Eng Struct Dynam. 32(4):597–605. doi:10.1002/eqe.240

Vahdani R, Gerami M, Vaseghi-Nia MA. 2019. The spectra of relative input energy per unit mass of structure for Iranian earthquakes. Intern J Civil Eng. 17(7):1183–1199. doi:10.1007/s40999-018-0377-x

Vanmarcke EH. 1975. On the distribution of the first-passage time for normal stationary random processes. J Appl Mech. 42(1):215–220. doi:10.1115/1.3423521

Wang X, Rathje EM. 2016. Influence of peak factors on site amplification from random vibration theory based site-response analysis. Bull Seismol Soc Amer. 106(4):1733–1746. doi:10.1785/0120150328

Zhang HZ, Deng J, Zhao YG. 2023. Damping modification factor of pseudo-acceleration spectrum considering influences of magnitude, distance and site conditions. Earthq Struct. 25(5):325–342.

Zhang HZ, Zhao YG. 2022. Effects of magnitude and distance on spectral and pseudo spectral acceleration proximities for high damping ratio. Bull Earthq Eng. 20(8):3715–3737. doi:10.1007/s10518-022-01328-9

Zhang HZ, Zhao YG. 2023. Estimation of input energy spectrum from pseudo-velocity response spectrum incorporating the influences of magnitude, distance, and site conditions. Eng Struct. 274:115165. doi:10.1016/j.engstruct.2022.115165

Appendices

Appendix A

Table A1. Coefficients of Eq. (16). Damping ratio range: $0.2 < \xi \leq 0.5$.

Site class	ζ	a_1	a_2	b_1	b_2	c_1	c_2
B	0.00258	−1.8733	1.3224	0.2722	−0.4914	3.0157	−1.2522
	0.00261	−2.0289	1.5323	0.3681	−0.4803	3.4544	−1.2827
	0.00266	−2.2573	1.8701	0.5397	−0.5579	4.2056	−1.6259
	0.00819	−1.2231	1.4384	0.2015	−0.5096	2.2974	−1.2983
	0.00648	−0.9383	1.4124	−0.0888	−0.3444	1.4819	−0.7048
	0.00775	−1.2871	1.7071	0.1124	−0.4057	2.5236	−1.1572
	0.01804	−0.3031	1.1907	−0.3268	−0.2479	0.4563	−0.3494
	0.02216	−0.6644	1.4249	−0.0494	−0.2994	1.4368	−0.5774
	0.02542	−0.4427	1.4626	−0.0358	−0.2751	1.1632	−0.3052
C	0.00306	−2.229	1.5711	0.5166	−0.5467	3.9643	−1.6178
	0.00285	−2.043	1.5824	0.3891	−0.4965	3.5123	−1.3546
	0.00332	−2.2504	1.8343	0.5506	−0.5265	4.2008	−1.5412
	0.00470	−0.8372	1.3333	0.139	−0.4649	1.4787	−1.0097
	0.01023	−0.8357	1.4597	−0.1278	−0.3231	1.3472	−0.8143
	0.01034	−1.0593	1.6131	0.107	−0.344	1.871	−0.7552
	0.01307	−0.4617	1.3787	−0.124	−0.2706	0.9458	−0.6097
	0.03256	−0.316	1.3453	−0.2142	−0.2386	0.6165	−0.4422
	0.03865	−0.3457	1.4256	−0.1565	−0.2053	0.7984	−0.3352
D	0.00441	−2.1366	1.755	0.5106	−0.535	3.9431	−1.7264
	0.00475	−2.3092	1.9275	0.6305	−0.5654	4.5365	−1.8725

(*Continued*)

Table A1. Continued.

Site class	ζ	a_1	a_2	b_1	b_2	c_1	c_2
	0.00475	−2.3766	2.1328	0.6716	−0.5875	4.6769	−1.9807
	0.01469	−0.63	1.4353	−0.2115	−0.2974	1.0185	−0.9508
	0.01349	−1.0956	1.6824	0.156	−0.386	1.9539	−1.0628
	0.01268	−1.0632	1.8427	0.2115	−0.4273	1.9876	−1.1632
	0.05414	−0.4121	1.3358	0.1825	−0.3833	1.3063	−0.767
	0.04487	−0.4721	1.4527	−0.1122	−0.208	1.0701	−0.4826
	0.05566	−0.1363	1.553	−0.2475	−0.1995	0.3984	−0.5231
E	0.04892	−1.3232	1.7245	0.0878	−0.47	2.1318	−1.6445
	0.05071	−1.5873	1.9826	0.2397	−0.5208	2.8826	−1.9713
	0.05553	−1.2708	2.0558	0.368	−0.6172	2.3224	−1.9657
	0.08133	−0.5523	1.6688	−0.2641	−0.319	0.9349	−1.3849
	0.07701	−0.5181	1.7727	−0.2993	−0.2746	0.8473	−1.2274
	0.08564	0.0584	1.719	−0.6102	−0.167	−0.4245	−0.9077
	0.10089	0.3185	1.2031	−0.5507	−0.0971	−0.6459	−0.3941
	0.11239	−0.2562	1.6016	−0.1762	−0.2239	0.8098	−1.0162
	0.12515	0.3278	1.5174	−0.4557	−0.1159	−0.4286	−0.4626

Appendix B

Table B1. Coefficients of Eq. (16). Damping ratio range: $0.05 \leq \xi \leq 0.2$.

Site class	ζ	a_1	a_2	b_1	b_2	c_1	c_2
B	0.00258	4.928	0.7317	−4.62	0.0047	−7.262	−0.6347
	0.00261	6.24	0.7835	−6.03	0.1883	−9.734	−0.3605
	0.00266	6.858	1.0179	−6.658	0.2123	−9.848	−0.5777
	0.00819	7.448	0.204	−3.148	0.0411	−8.404	0.2719
	0.00648	8.538	0.0846	−4.018	0.2544	−10.514	1.0076
	0.00775	9.154	0.2455	−4.464	0.3121	−11.402	0.8616
	0.01804	6.818	0.2046	−2.1	−0.0099	−4.924	0.35
	0.02216	6.28	0.4174	−1.262	−0.0868	−2.904	0.0938
	0.02542	6.112	0.4823	−1.036	−0.0991	−2.08	0.2531
C	0.00306	8.868	0.441	−6.844	0.2641	−16.118	0.2392
	0.00285	7.52	0.632	−6.428	0.2457	−12.55	0.0128
	0.00332	9.336	0.688	−7.766	0.368	−16.006	0.2016
	0.00470	7.798	0.0203	−3.162	0.1576	−9.504	0.8014
	0.01023	7.082	0.2667	−2.668	0.139	−6.962	0.5847
	0.01034	7.63	0.3319	−2.614	0.1821	−6.812	0.6621
	0.01307	3.684	0.6937	0.56	−0.3175	3.442	−0.7636
	0.03256	4.276	0.5974	0.152	−0.2262	1.764	−0.3984
	0.03865	4.33	0.7038	0.348	−0.2377	2.186	−0.4217
D	0.00441	11.058	0.2433	−7.902	0.4833	−20.234	0.9144
	0.00475	10.816	0.455	−7.936	0.455	−19.244	0.6456
	0.00475	12.464	0.4536	−9.04	0.5707	−22.794	0.9828
	0.01469	9.102	−0.0799	−3.726	0.3482	−12.146	1.292
	0.01349	8.27	0.3169	−2.914	0.1944	−9.256	0.6877
	0.01268	9.908	0.2052	−3.958	0.3571	−12.768	1.2037
	0.05414	5.186	0.4254	−0.406	−0.1929	−1.072	−0.1884
	0.04487	5.218	0.5762	−0.322	−0.1347	−0.672	−0.1059
	0.05566	5.464	0.6157	−0.064	−0.1308	−0.332	−0.0942
E	0.04892	11.97	−0.0543	−7.178	0.5625	−21.89	1.5959
	0.05071	14.59	−0.1167	−8.914	0.7305	−27.832	2.0095
	0.05553	16.196	−0.3571	−9.828	0.9507	−30.908	2.6811
	0.08133	8.732	0.1682	−2.946	0.2421	−11.006	0.8131
	0.07701	8.814	0.2711	−2.648	0.2377	−9.942	0.8021
	0.08564	9.368	0.1565	−2.75	0.3568	−10.944	1.243
	0.10089	6.744	0.1118	−1.222	0.1463	−5.242	0.7264
	0.11239	4.454	0.7504	0.562	−0.2208	1.306	−0.677
	0.12515	6.006	0.5948	−0.152	−0.0878	−1.874	0.0063